Inorganic Chemistry

Article

pubs.acs.org/IC

Precession Electron Diffraction Tomography for Solving Complex Modulated Structures: the Case of $Bi_5Nb_3O_{15}$

Philippe Boullay,*[,†] Lukas Palatinus,[‡] and Nicolas Barrier[†]

[†]Laboratoire CRISMAT, UMR CNRS 6508, ENSICAEN, 6 Bd Maréchal Juin, F-14050 Caen Cedex 4, France

[‡]Institute of Physics of the AS CR, v.v.i. Na Slovance 2, 182 21 Prague, Czechia

Supporting Information

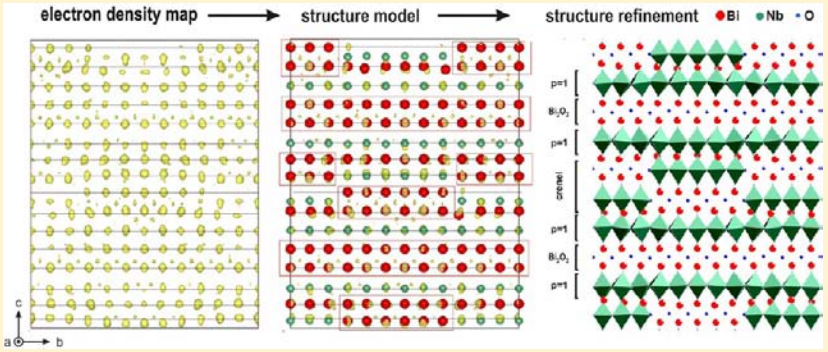

ABSTRACT: The crystal structure of the 1D incommensurately modulated phase $Bi_5Nb_3O_{15}$ [superspace group $X2mb(0b0)000$, a = 5.46781(7) Å, b = 5.47381(8) Å, c = 41.9005(5) Å, and $\mathbf{q}$ = 0.17588(8)$\mathbf{b}^*$] is solved by electron diffraction using a tomography technique combined with precession of the electron beam. The (3 + 1)D structure is further validated by a refinement against powder X-ray diffraction (PXRD). A coherent picture of the true nature of this compound is obtained, conciliating experimental observations made by different groups using transmission electron microscopy and PXRD. $Bi_5Nb_3O_{15}$ does not have a mixed-layer Aurivillius-type structure but does contain structural elements, $[Bi_2O_2]^{2+}$ slabs, and perovskite-like blocks, characteristic of Aurivillius phases. The presence of aperiodic crystallographic shear planes (CSPs) along the modulated direction $\mathbf{b}$ leads to the formation of an original layered structure containing both continuous and discontinuous $[Bi_2O_2]^{2+}$ and perovskite-like octahedral layers. Between CSPs, the stacking of these two structural elements exhibits an unprecedented nonuniform sequence referring to Aurivillius phases.

INTRODUCTION

The structures of bismuth-layered oxides from the Aurivillius family[1] are usually described as resulting from the regular stacking of $[Bi_2O_2]^{2+}$ slabs and perovskite-like $[A_{p-1}B_pO_{3p+1}]^{2-}$ blocks (Figure 1a). The integer p corresponds to the number of sheets of corner-sharing BO_6 octahedra forming the perovskite blocks, where the A site can be occupied by large 12-fold-coordinated cations such as Na^+, K^+, Ca^{2+}, Sr^{2+}, Ba^{2+}, Pb^{2+}, Bi^{3+}, or Ln^{3+} and the B site by 6-fold-coordinated cations such as Ti^{4+}, Nb^{5+}, or W^{6+}. "Mixed-layer" compounds also exist (Figure 1b), where perovskite blocks of size p and p + 1 are separated by the $[Bi_2O_2]$ slabs distributed along the stacking direction.[2] A large number of Aurivillius phases exhibit ferroelectric (FE) properties at room temperature and are known to be nonpolar tetragonal at high temperature with space group $I4/mmm$ for the archetypal paraelectric phase. For the FE Aurivillius phases, the structure observed at room temperature presents usually three distortions from the archetypal structure:[3] a tilting of the octahedra around the a axis, a rotation of the octahedra around the c axis, and atomic displacements along the polar a axis.

These structural features common to the FE Aurivillius phases lead to very predictable structures and space groups as shown using a (3 + 1)D superspace group approach, where Aurivillius-type compounds are considered as B-cation-deficient perovskites of the general formula $AB_{1-x}O_3$.[2,4,5] For a given composition x, the sequence of B vacancies, i.e., the occurrence of a $[Bi_2O_2]^{2+}$ slab in the stacking, is predictable and corresponds to a so-called "uniform sequence", where the vacancies tend to be separated as far as possible. In the case of mixed-layer compounds, it is also predicted that the existence of two perovskite-type blocks, with an odd and even numbers of octahedral layers combined with the specific rotation of the octahedra, imposes one to consider 2 times the p and p + 1 blocks to obtain the periodicity along the c axis. Likewise, the a and b parameters should be close to $a \approx b \approx a_p\sqrt{2}$, where a_p (≈3.9 Å) represents the perovskite subcell. As a direct consequence, these FE mixed-layer Aurivillius phases should possess a body-centered lattice, while an A- and B-centered lattice is expected, respectively, for even- and odd-layer FE Aurivillius phases.

Known for decades,[7] the phase $Bi_5Nb_3O_{15}$ has been first considered as one of these mixed-layer compounds that would

Received: February 28, 2013
Published: May 1, 2013

   dx.doi.org/10.1021/ic400529s | *Inorg. Chem.* 2013, 52, 6127−6135

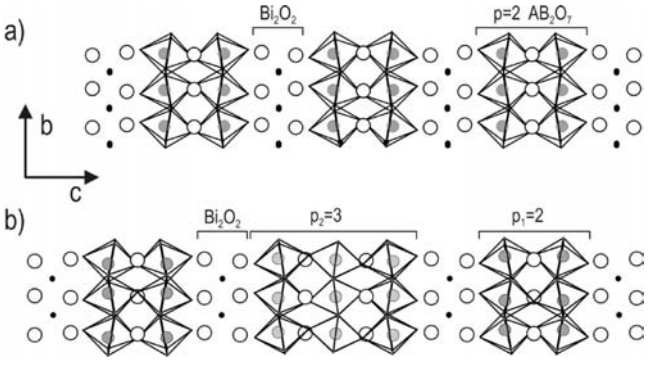

Figure 1. *y*0*z* projection of the schematic structures of (a) even- and (b) mixed-layer Aurivillius compounds. $[Bi_2O_2]^{2+}$ slabs and perovskite-like $[A_{p-1}B_pO_{3p+1}]^{2-}$ blocks regularly alternate along the stacking direction *c*.

be related to $Bi_5Ti_{1.5}W_{1.5}O_{15}$[8] and $Bi_5TiNbWO_{15}$,[9] whose structures were recently refined from powder diffraction data in the space group *I*2*cm* (No. 46). These mixed-layer Aurivillius phases correspond, in a first approximation, to a regular intergrowth of the corresponding "simple" Aurivillius phases with p = 1 and 2. Compared to other mixed-layer phases, $Bi_5Nb_3O_{15}$ is yet particular because the p = 1 ($[Bi_2NbO_6]^-$) and p = 2 ($[Bi_3Nb_2O_9]^+$) parts of the intergrowth are not neutral and do not exist as single-phase materials. Moreover, $Bi_5Nb_3O_{15}$ has been identified as having a 1D incommensurately modulated structure, and an approximate structural model incorporating a steplike dislocation has been proposed, basing on transmission electron microscopy (TEM) investigations.[10−13] Nonetheless, all of the crystallographic investigations using either X-ray or neutron diffraction[14] eluded this specificity, and no structural model taking into account the incommensurate nature of this compound has been refined. In the present work, the incommensurately modulated structure of $Bi_5Nb_3O_{15}$ is solved ab initio using a technique called electron diffraction tomography (EDT)[15] combined with precession electron diffraction (PED).[16] The (3 + 1)D structure is further refined against powder X-ray diffraction (PXRD) data.

EXPERIMENTAL SECTION

Polycrystalline samples of $Bi_5Nb_3O_{15}$ were prepared by a solid-state reaction. Stoichiometric amounts of Bi_2O_3 and Nb_2O_5 were mixed, pressed into pellets, and heated at 1000 °C for 10 h. After grinding, the obtained powder was used for a preliminary characterization using X-ray diffraction, indicating formation of the $Bi_5Nb_3O_{15}$ phase (PDF2 card 01-077-3967[14]). For TEM investigations, a small quantity of the powder was crushed in an agate mortar to obtain small fragments that were put in a suspension in alcohol. A drop of the suspension was then deposited and dried on a copper grid with a thin film of amorphous carbon.

The PXRD pattern used for structure refinement was collected on a Bruker D8 diffractometer using Cu Kα_1 radiation (1.54056 Å), selected by an incident germanium monochromator, and equipped with a Lynx-Eye detector. A beam knife was used to reduce X-ray diffusion at low angles. The X-ray diffraction pattern was recorded in an angular range between 5° and 110° (2θ) with a scan step of 0.008° (2θ).

The electron diffraction data were collected on a part of a larger crystal. First, oriented diffraction patterns were collected to assess the quality of the selected crystal using selected-area PED (SA-PED; Figure 2a). EDT data (Figure 2b) were collected on a transmission electron microscope CM120 at an accelerating voltage of 120 kV equipped with an upper-mounted CCD camera Olympus Veleta with a dynamic range of 14 bits. The tilt range was from −45 to +42°. This data set was collected in a semiautomatic mode, where all actions during the data collection (sample tilt, exposure of the diffraction

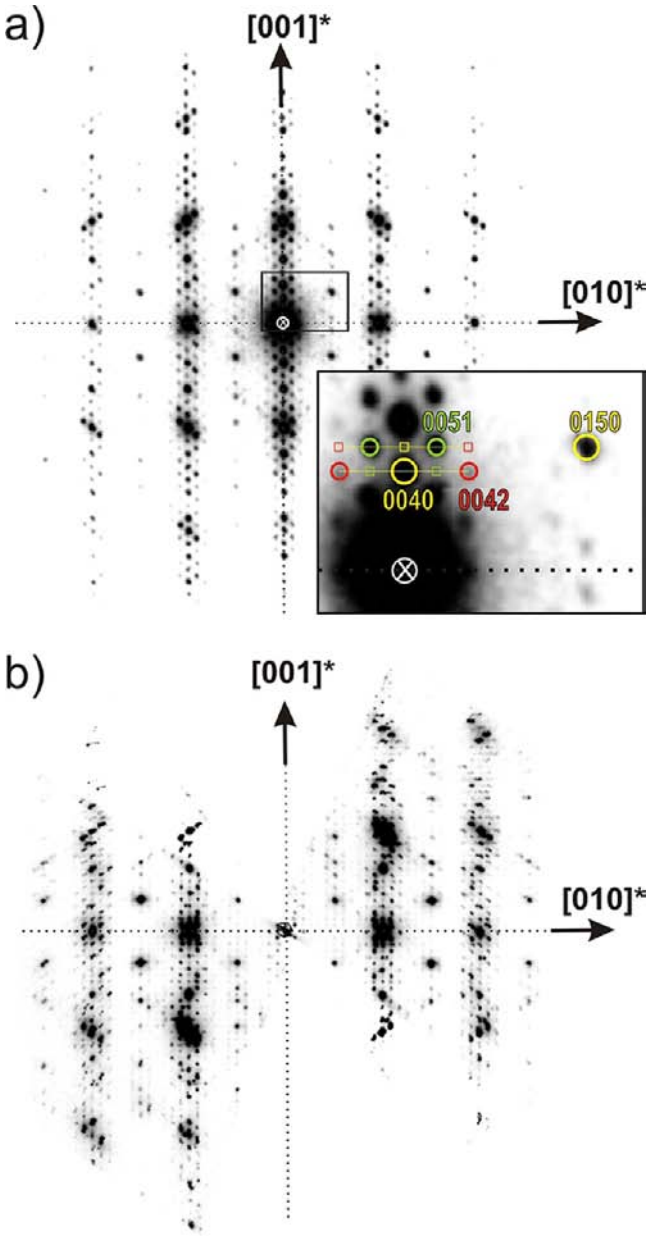

Figure 2. (a) [100] zone axis patterns obtained by SA-PED with an inset showing indexation with condition 0*klm*: $k + l + m = 2n$. (b) 0*kl* reciprocal space section reconstructed from the EDT experiment obtained by microdiffraction PED on the same crystal. In both cases, the precession angle is 1.2°.

pattern, switching from diffraction to imaging mode, etc.) are performed automatically by a computer program. The operator only checked the position of the crystal after each exposure and shifted the crystal, if necessary. The data were collected in microdiffraction mode with a beam-size diameter of 0.4 μm and with a precession angle of 1.2°. Larger precession angles were avoided to prevent overlap of neighboring reflections. The data set yielded a data completeness of over 90% (total number of reflections in the 0.9 Å resolution shell), sufficient for the structure solution process.

The raw electron diffraction data were processed using the programs *PETS*[17] and *Jana2006*.[18] The procedure is described in detail elsewhere.[19] *PETS* is used to perform peak picking in the diffraction patterns and to refine the optimum orientation of the rotation axis in the diffraction patterns (which is not known exactly in electron diffraction experiments). *PETS* performs also a difference vector space analysis to produce a more complete representation of the

dx.doi.org/10.1021/ic400529s | *Inorg. Chem.* 2013, 52, 6127−6135

Table 1. Results of the Rietveld PXRD (3 + 1)D Refinement of $Bi_5Nb_3O_{15}$ with Fractional Coordinates and Amplitudes of the Displacive Functions (s for sinus and c for cosinus)[a]

SSG	Z	a (Å)	b (Å)	c (Å)	β (deg)	volume (Å^3)
$X2mb(0\beta0)000$	4	5.46781(7)	5.47381(8)	41.9005 (5)	0.17588(8)	1254.04(7)
		overall		main refln		sat. order 1
no. of reflns				870		1568
R_{obs}/wR_{obs}		4.85/6.12		4.43/6.36		5.21/6.01
Rietveld param		R_p = 7.49		wR_p = 10.51		GOF = 2.26

	Bi3	Bi4	Nb1	Nb2	O10	O11
x_4/Δ	0.5/0.5	0.5/0.5	0/0.5	0/0.5	0/0.5	0/0.5

	x	y	z		x	y	z
Bi1	0.258(7)	0.25	0.65669(14)	O1	0.004(5)	0.0001(10)	0.1005(3)
s,1	0	−0.0820(18)	0	s,1	−0.051(3)	−0.042(3)	0.0033(4)
c,1	0.046(2)	0	0.00355(18)	c,1	0.007(3)	0	0.0030(4)
Bi2	0.752(7)	0.75	0.65742(16)	O2	0.504(5)	0.0003(10)	0.1017(3)
s,1	0	−0.0746(18)	0	s,1	−0.047(3)	0.038(3)	0.0030(4)
c,1	0.019(3)	0	0.00999(17)	c,1	0.006(3)	0	0.0025(4)
Bi3	0.251(6)	0.25	0.7754(2)	O3	0.507(6)	−0.0004(10)	0.6979(3)
s,1	0	−0.031(3)	0	s,1	−0.005(2)	−0.008(2)	−0.0014(3)
c,1	−0.002(2)	0	0.0007(3)	c,1	0	0.0025(11)	−0.0018(2)
Bi4	0.769(6)	0.75	0.7749(2)	O4	0.005(6)	0.0003(10)	0.6972(3)
s,1	0	−0.019(3)	0	s,1	0	−0.0112(16)	−0.0014(3)
c,1	0	0	0.0007(5)	c,1	−0.0026(17)	0.0017(14)	−0.0023(2)
Bi5	0.754(6)	0.25	−0.03040(15)	O5	0.762(6)	0.75	0.8512(2)
s,1	0	0.0543(14)	0	s,1	0	0.021(5)	0
c,1	−0.019(3)	0	0.00172(19)	c,1	0	0	−0.0037(3)
Bi6	0.243(6)	0.75	−0.02969(15)	O6	0.249(6)	0.25	0.8511(2)
s,1	0	0.0086(14)	0	s,1	0	−0.018(4)	0
c,1	−0.011(3)	0	0.00031(18)	c,1	0.010(4)	0	−0.0040(3)
Nb1	0.244(6)	0.25	0.7960(3)	O7	0	0	0
s,1	0	0.022(5)	0	s,1	0	0	−0.0043(5)
c,1	0	0	0.0045(7)	c,1	0	0	0
Nb2	0.761(6)	0.75	0.7955(3)	O7b	0.510(3)	0.5	0
s,1	0	0.022(5)	0	s,1	0	0	0.0033(5)
c,1	−0.008(8)	0	0.0024(7)	c,1	0	0	0
Nb3	0.759(5)	0.25	0.59799(19)	O8	0.749(4)	0.25	0.0507(2)
s,1	0	−0.027(2)	0	s,1	0	−0.040(5)	0
c,1	0	0	−0.0016(2)	c,1	0	0	0.0010(3)
Nb4	0.743(5)	0.25	0.09772(18)	O9	0.260(4)	0.75	0.0504(2)
s,1	0	0.009(2)	0	s,1	0	0.041(5)	0
c,1	0.017(3)	0	0	c,1	0	0	0.0012(3)
O10	0.253(7)	0.25	0.7499(3)	O11	0.760(7)	0.75	0.7491(3)
s,1	0	0	0	s,1	0	0	0
c,1	0	0	0.0033(8)	c,1	0	0	0.0009(6)

[a]The center x_4 and length Δ of the crenel functions are indicated when used. Isotropic thermal displacement parameters (U_{iso}) are fixed to 0.025 Å^2 for the O atom and 0.005 Å^2 for the Nb atom and refined to 0.0145(4) Å^2 for the Bi atom.

reciprocal lattice (see Kolb et al.[20]). The indexing utility of *Jana2006* was then used to find and refine the orientation matrix, the unit cell parameters, and the primary modulation vector (see details below) from the list of peak coordinates. Using the refined orientation matrix, *PETS* allows integration of the reflection intensities in diffraction patterns using (3 + 1)D indexing. The result of the procedure was a list of *hklm* indices with associated intensities and estimated standard deviations based on counting statistics. On the ∼12000 measured reflections, about 2250 independent reflections were observed, with $I > 3\sigma(I)$ leading to R_{int} of 21.4 and a redundancy of 1.8. Such values would be considered poor for X-ray diffraction data but are reasonable for electron diffraction data.

CRYSTAL STRUCTURE DETERMINATION

As indicated in previous TEM studies (see Zhou et al.[10,11] and Ling et al.[12,13]), while $Bi_5Nb_3O_{15}$ was clearly identified as an incommensurately modulated phase with an average cell corresponding to $a \approx b \approx a_p\sqrt{2}$ and $c \approx 10a_p$, a certain variability of the modulation vector was found with the apparent existence of one orthorhombic variant with $\mathbf{q} \approx (1/6)\mathbf{b}^*$[11] and one monoclinic variant with $\mathbf{q} \approx 0.04\mathbf{a}^* + 0.18\mathbf{b}^* + \mathbf{c}^*$.[13]

In the present study, analysis of the electron diffraction patterns (both oriented and from the tilt series) indicated that the structure is orthorhombic and incommensurately modulated with a modulation vector $\mathbf{q} = 0.0011(12)\mathbf{a}^* + 0.1758(6)\mathbf{b}^* + 0.0054(89)\mathbf{c}^*$ refined using the list of peak coordinates obtained from the PED tomography experiment and considering the nonstandard centering $X = (^1/_2, ^1/_2, ^1/_2, ^1/_2)$. Because the accuracy of the cell parameters determined from electron diffraction data is inferior to the results from powder diffraction data, we used the cell parameters refined from the

dx.doi.org/10.1021/ic400529s | Inorg. Chem. 2013, 52, 6127−6135

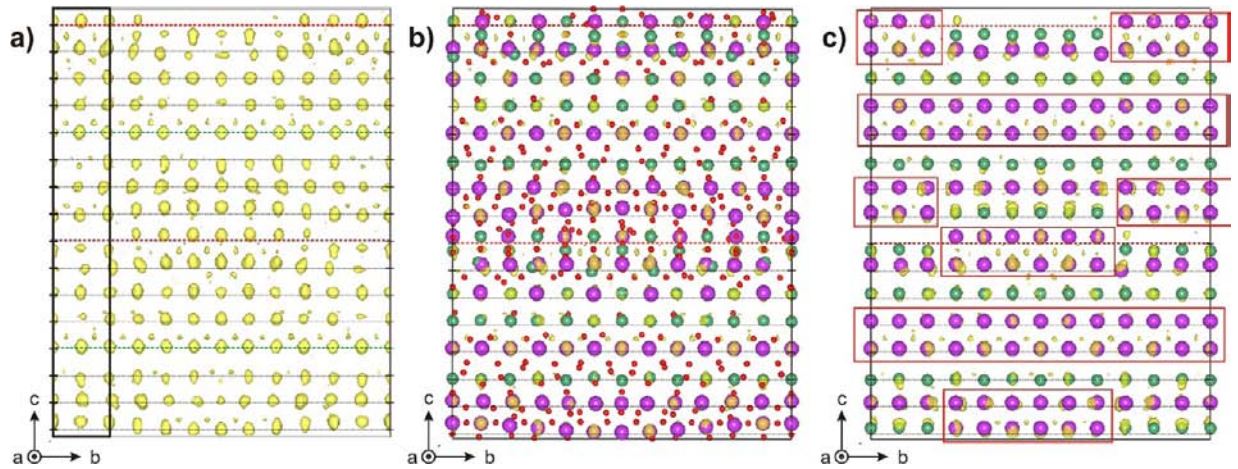

Figure 3. (a) [100] projection of the electron density map generated by *Superflip* as an output of the charge-flipping structure solution procedure. The basic unit cell is multiplied by 6 along the modulated direction. (b) Raw solution obtained from *Superflip* superimposed to the electron density map. Bi, Nb, and O atoms are represented in violet, green, and red, respectively. (c) Cationic structural model obtained after interpretation of the electron density map and the addition of discontinuous functions (crenels). The $[Bi_2O_2]$ slabs are outlined in red.

PXRD data (see Table 1). Additional systematic absences of the form $hk0m$: $k = 2n$ indicated a glide plane b perpendicular to **c**. However, analysis of the systematic absences was not very conclusive because of the possibility of overlaps and the small number of affected reflections. The structure solution was performed in a (3 + 1)D superspace using the program *Superflip*,[21] assuming kinematical diffraction intensities. The result of the structure solution is a (3 + 1)D superspace electron density. The structure solution proceeds without forcing the symmetry onto the solution so that the resulting density can be analyzed for symmetry. The symmetry analysis of the solution[22] indicated the superspace group $Xmm2(0b0)$-000. The b-glide plane perpendicular to **c** appeared much less probable than the mirror planes (symmetry agreement factor between 30 and 40, in contrast to the values below 10 for the mirror planes) but could not be entirely excluded given the fact that electron diffraction data are very noisy by the measure of structure solution procedures adapted to X-ray diffraction data. Finally, we decided to interpret the structure using the symmetry $Xmm2(0b0)000$ and to check for the presence of the b-glide once again in the later stages of structure analysis.

The output of the charge-flipping procedure is a scattering density map (electrostatic potential in the current case) that can be interpreted in terms of atomic positions by *Jana2006*. If the structure is incommensurately modulated, the scattering density is described in superspace, and *Jana2006* locates in the density not only the atomic positions but also the modulation functions. However, the interpretation is limited to first-harmonic continuous modulation functions and cannot therefore correctly interpret more complicated modulations, especially discontinuous ones.

The solution is represented in Figure 3a as a [100] projection using a 6-fold supercell along the modulated direction **b** [$\mathbf{q} \approx (1/6)\mathbf{b}^*$]. Taking into account the scattering powers of Bi, Nb and O, a reasonable hypothesis is to assume that the heavy Bi and Nb scatterers shall dominate the density map. As a guide to the eyes, the horizontal dotted lines in Figure 3a represent the average periodicity expected for the cation-containing layers $[BiO]_\infty$ and $[NbO_2]_\infty$. With $Bi_5Nb_3O_{15}$ being supposedly related to a 1 + 2 mixed-layer Aurivillius phase,[8,9] 16 of such layers are expected along the stacking direction **c**. Along the modulation direction **b**, two symmetry-related layers (highlighted in red in Figure 3a) appear clearly discontinuous with density located either above or below the reference line with a sharp, steplike transition. In the layers far from this part of the structure, strong density nodes lie on the reference lines without noticeable variations of the position along z (see green lines in Figure 3a).

Figure 3b shows the atomic positions as interpreted by *Jana2006*. Clearly, the discontinuous layers and their surroundings are poorly described, and extra cationic layers are present. However, these discontinuities are clearly visible in the x_3-x_4 and x_2-x_4 sections through the electrostatic potential reconstructed by *Superflip* (Figure 4a,c,d). These sections are calculated at such positions as to contain the atomic positions near the red line in Figure 3a. For these positions, crenel (steplike) functions were introduced to better account for the observed modulation. Legendre polynomials were introduced to account for additional positional modulations of the atoms within the crenel intervals. The atomic positions lying close to the green lines in Figure 3a can be satisfactorily described by a continuous modulation function (Figure 4b,e).

After introduction of the crenel functions based on the observed Fourier maps, the cationic structural model in Figure 3c was obtained. Interestingly, the O-atom positions corresponding to the $\square O_2$ layers of the $[Bi_2O_2]$ slabs are clearly visible in the electron density maps and were thus introduced in the model. This partial model was then refined against the PED data. The remaining O-atom positions were then introduced by examination of the difference Fourier maps to complete the coordination polyhedra of the cations.

At this stage of structure analysis, we decided to check the presence of the b-glide plane perpendicular to **c** using the symmetry-checking option in *Superflip*.[22] Because the O atoms contribute very little to the overall electrostatic potential and, moreover, their exact positions are not very accurately determined, we considered only the cationic sublattice in the test. The symmetry agreement factor below 10% indicates that this symmetry element is most probably present in the structure. $Bi_5Nb_3O_{15}$ is known in the literature to be FE at room temperature.[23,24] Therefore, one of the two mirror-plane symmetries must be broken. The symmetry breaking is very subtle, and the accuracy of the data (electron or powder diffraction) is not sufficient to determine the polar axis. In

dx.doi.org/10.1021/ic400529s | *Inorg. Chem.* 2013, 52, 6127−6135

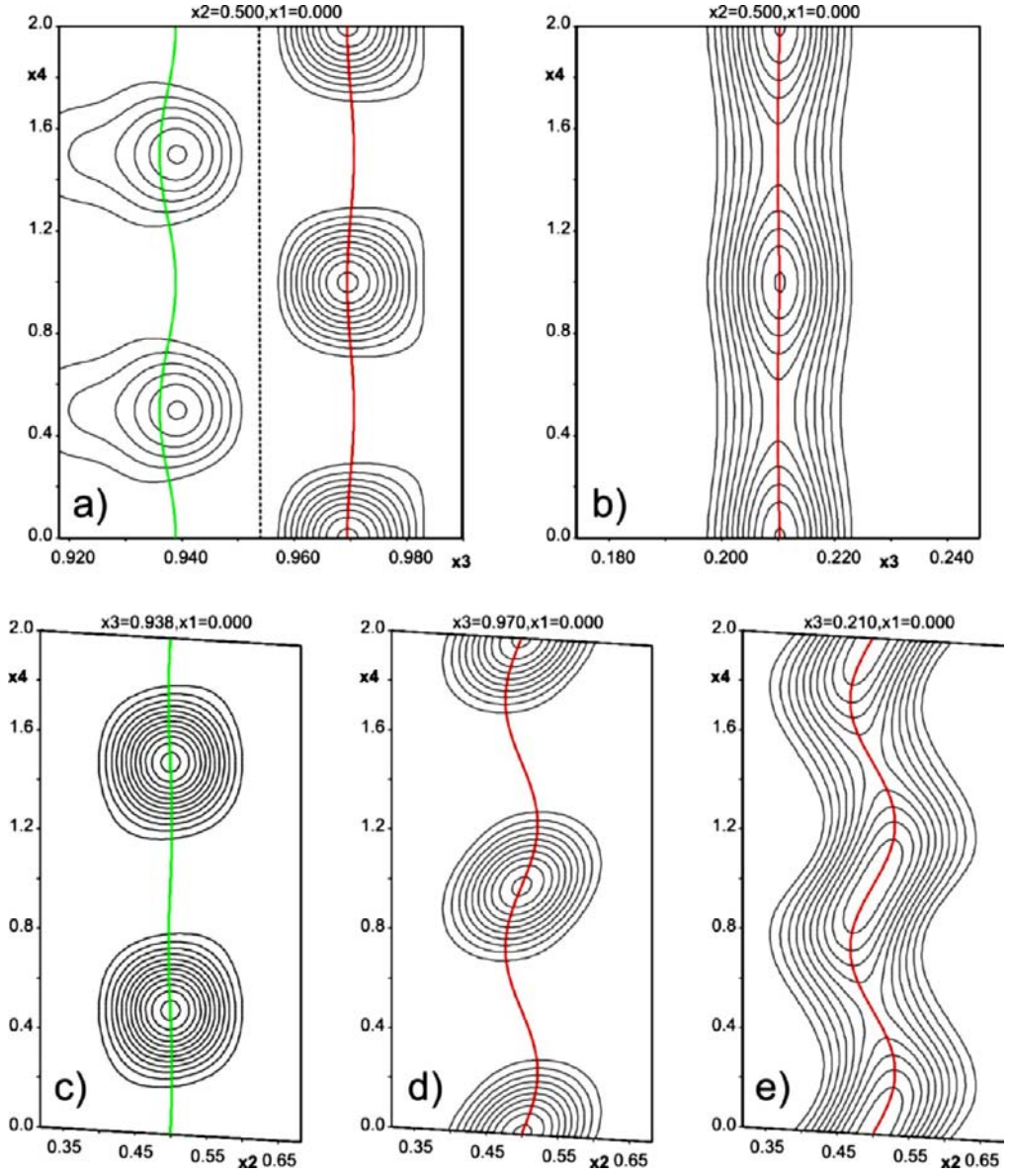

Figure 4. x_3−x_4 sections obtained at (a) $z \sim 0.95$ and (b) $z \sim 0.21$, i.e., at the red and green dotted lines in Figure 3a, respectively. x_2−x_4 sections obtained for parts c and d in the vicinity of the red dotted lines in Figure 3a and showing discontinuous atomic domains. In part e, the x_2−x_4 section at green dotted lines in Figure 3a shows a continuous atomic domain. Continuous atomic domains corresponding to the raw interpretation of the solution proposed by *Jana2006* are represented by red and green lines for Bi and Nb atoms, respectively.

agreement with the trend observed in related polar Aurivillius phases, we assume that the polar axis is **a**. The resulting superspace group is then $X2mb(0b0)000$ [standard setting $I2cm(00g)0s0$, number 46.1.12.8 in the superspace group tables by Stokes et al.[25]].

The amount of information provided by electron[11,13] and powder diffraction[14] is strikingly different in terms of the number of observable satellite reflections. The difference is so large that a question could be raised of whether the crystal chosen for the tomography experiment is representative of the bulk material used for the powder diffraction experiment. The question can be answered by refining the structure model against PXRD data. The Rietveld refinement of the structure model reproduced quite well the observed pattern, i.e., strong peaks associated with the average structure as well as sparse weak satellite peaks (Figure 5). The diffraction signal of O atoms is weak, and the PED data did not allow a robust unrestrained refinement of all parameters. The situation was even worse in the Rietveld refinement against PXRD data. To maintain a reasonable geometry of the NbO_6 octahedra, we imposed soft restraints on 43 O−O and 16 Nb−O distances. In *Jana2006*, the $\sigma(d)$ value is used to derive the weight of the distance restraint in the minimized sum used in the refinement, in analogy with $\sigma(I)$ for intensities. If a distance restraint is not in conflict with the refinement, it will go close to the central value (2.80 ± 0.05 Å for O−O and 1.90 ± 0.05 Å for Nb−O). In the opposite way, it will just tend to go closer to the limit.

Having two structure refinements against two different data sets, another question emerges, namely, which refinement would be more reliable? In terms of clarity of the model, the PED data are certainly more informative. Only the PED data allow localization of the O atoms. However, the PED data are biased by the dynamical diffraction effects still present even using the precession method and leading here to values of the

dx.doi.org/10.1021/ic400529s | *Inorg. Chem.* 2013, 52, 6127−6135

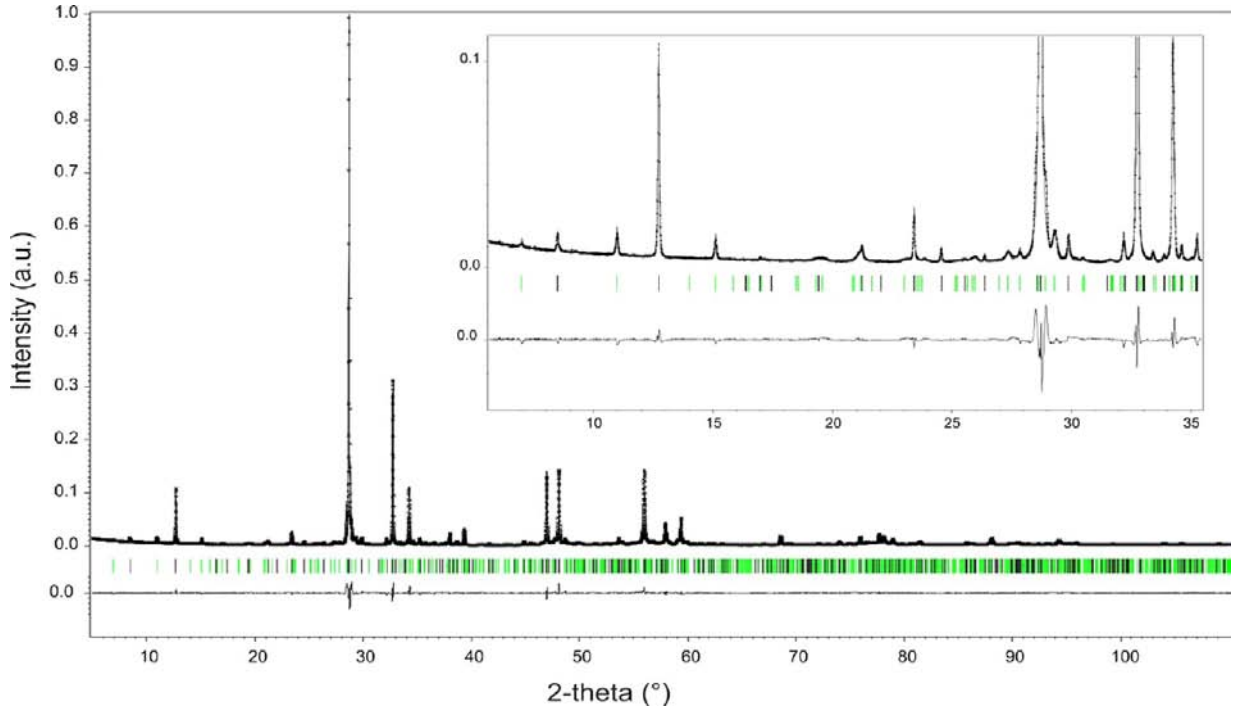

Figure 5. Final observed, calculated, and difference plots obtained for the PXRD Rietveld refinement of $Bi_5Nb_3O_{15}$. The black tick marks indicate the main reflections and the green set the satellite reflections, as considered in the (3 + 1)D approach.

reliability factors (R_{obs} and wR_{obs}) of around 30%. The Rietveld refinement must be restrained to be stable, but the kinematical diffraction model is appropriate. For this reason, we decided to present the results of the Rietveld refinement as the best available structure model. The results of the Rietveld refinement are presented in Table 1, and the [100] projection of the refined structure is represented in Figure 6. The result of the structure refinement against PED data is given as Supporting Information.

DISCUSSION

In agreement with the unrefined model based on the interpretation of high-resolution electron microscopy images,[11] our structure solution of $Bi_5Nb_3O_{15}$ contains structural motifs (layers) similar to the mixed-layer Aurivillius phases. Some of these layers are reduced to slabs with finite length along the modulation direction **b** by crystallographic shear planes (CSPs). As a result, the structure contains both continuous and discontinuous layers of NbO_6 octahedra along the modulated direction **b** (Figure 6). The discontinuous layers are predominantly made of six octahedra with occasional units of five octahedra in agreement with the modulation vector $\mathbf{q} = 0.17588(8)\mathbf{b}^* \in [{}^1/_6, {}^1/_5]$ being closer to ${}^1/_6$. Located between the continuous octahedral layers, these discontinuous octahedral blocks are attached, along **b**, once with the continuous layer above and next with the one below, forming $p = 2$ perovskite slabs arranged in a zigzag manner (Figures 6c and 7b). The result of this arrangement is the layer sequence of the type $|p = 1|p = 2|p = 2|p = 1|$ along **c**. Taking this sequence as the basic building unit (see the delimited area in Figure 6c), the structure can be seen as a result of the presence of CSPs along **b** applied to the basic building unit. It is most notable that the basic stacking sequence is nonuniform. Such a feature has never been observed in any mixed-layer Aurivillius phases reported to date, and this structure does not fit the unified description of Aurivillius phases,[2,4] where the uniform sequence associated with the "1 + 2" mixed-layer Aurivillius phase is unique and corresponds to $|p = 1|p = 2|p = 1|p = 2|$ (see illustration in Figure 6a). Clearly, $Bi_5Nb_3O_{15}$ cannot be seen just as a layered Aurivillius-type structure with periodic CSP. Keeping a uniform sequence of the octahedral layers stacking along **c**, such CSPs would lead to the formation of "collapsed" structures (see the schematic drawing in Figure 7c) quite similar to what is known in the high-T_c superconductors and related compounds.[26,27]

The octahedral tilting patterns were investigated on a broad range of Aurivillius phases.[28] It was shown that the octahedral tilting (and correlatively T_c) increases as the perovskite tolerance factor $t = (R_A + R_O)/\sqrt{2}(R_B + R_O)$ decreases. $Bi_5Nb_3O_{15}$, with a t value of 0.936 [$R_{O^{2-}} = 1.40$ Å, $R_{Nb^{5+}(VI)} = 0.64$ Å, and $R_{Bi^{3+}(XII)} = 1.30$ Å], is well below the lowest value reported for the Aurivillius phase with $t \sim 0.95$ in $CaBi_2Nb_2O_9$,[29] which possesses a pronounced octahedral tilting and high T_c. Neutron powder diffraction data would probably result in a more accurate description of the O-atom positions, but we believe that the present work provides a gross but largely correct picture of the octahedral tilting present in this compound. In the $Bi_5Nb_3O_{15}$ structure, the discontinuous octahedral layers as well as the part of the continuous layers attached to them present no significant octahedral tilting, notably around the **c** axis (see Figure 8). The largest octahedral tilting is present in the continuous octahedral layers close to the CSPs. Assuming a mechanism of FE polarization similar to that in conventional Aurivillius phases, one expects polarization along the direction around which the tilting of the octahedra takes place, i.e., perpendicular to the atomic displacements involved in the octahedra tiltings. In our structural model, although the tiltings are small, the main tilting of the octahedra is around the **a** axis (Figure 8a), in agreement with this expectation.

The Nb−O distances (Figure 9) are in the range of 1.8−2.3 Å with usually one short distance and one long distance related to

dx.doi.org/10.1021/ic400529s | Inorg. Chem. 2013, 52, 6127−6135

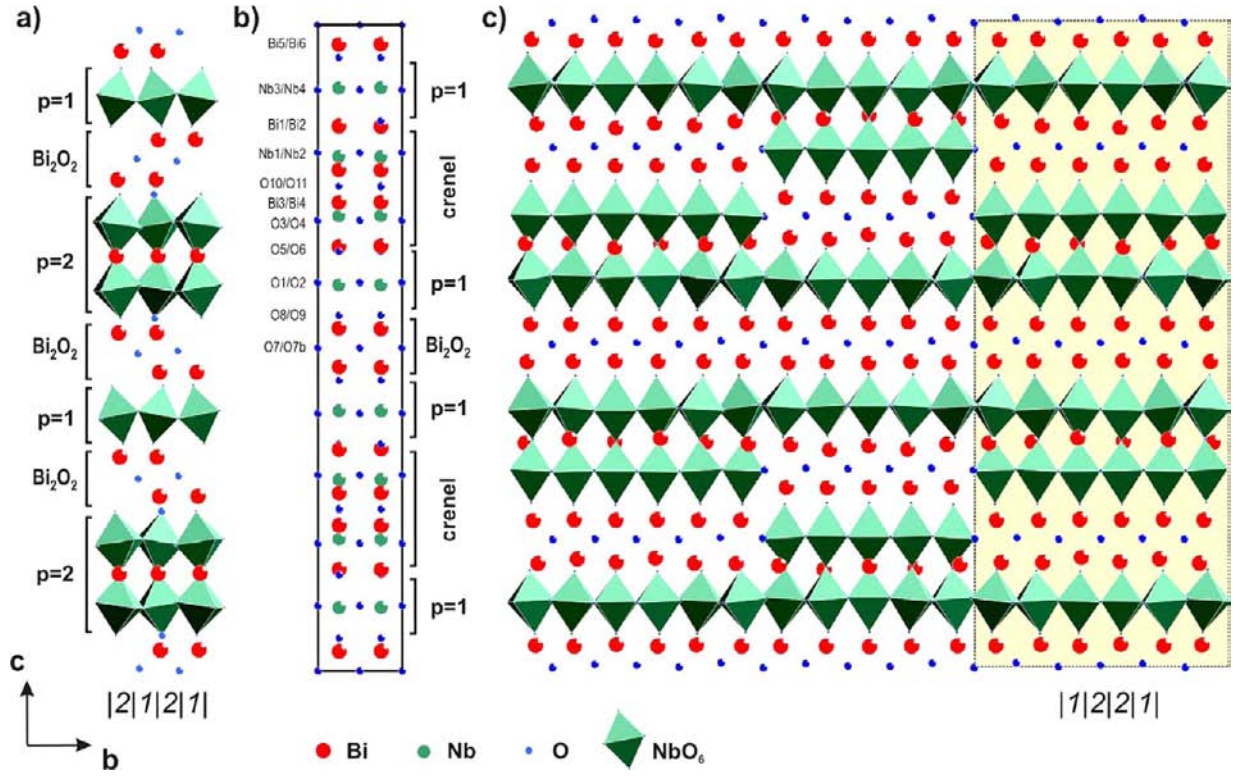

Figure 6. (a) Structure of the $n = 1 + 2$ intergrowth $Bi_5Ti_{1.5}W_{1.5}O_{15}$.[8] (b) Average structure of $Bi_5Nb_3O_{15}$. (c) Supercell along the modulated direction **b**, revealing a nonuniform stacking sequence |1|2|2|1| along **c** and the periodic "shear" both characteristic of this phase.

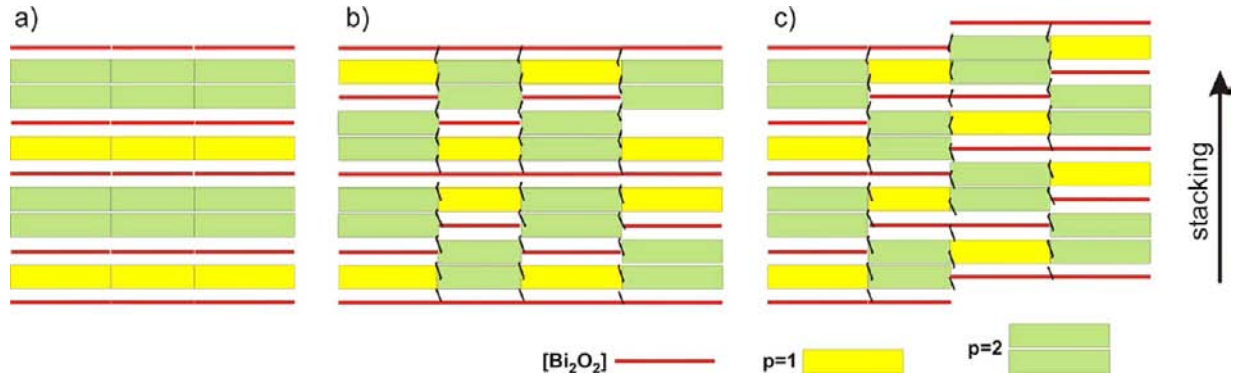

Figure 7. Schematic drawings: (a) A "1 + 2" mixed-layer Aurivillius phase,[8,9] with continuous octahedral layers alternating regularly along the stacking direction following the uniform sequence $|p = 1|p = 2|p = 1|p = 2|$. (b) $Bi_5Nb_3O_{15}$, where the stacking sequence is nonuniform $|p = 1|p = 2|p = 2|p = 1|$ with a periodic shear leading to the coexistence of both continuous octahedral layers and discontinuous octahedral blocks. (c) A "collapsed" phase, where the stacking sequence is identical with that of part a but with a periodic shear, leading to a structure made solely of discountinuous octahedral blocks.

apical O atoms. The Bi−O distances are more scattered with the shortest distances around 2.2 Å . The accuracy of the present structure determination is low, especially for O atoms, but this result is in agreement with expected values.

The small difference measured between the *a* and *b* lattice parameters is a signature of low octahedral tilting in layered Aurivillius phases.[6,29−31] $Bi_5Nb_3O_{15}$ certainly exhibits less octahedral tilting than what would be expected for a layered Aurivillius phase with such a low *t* value. This might be the reason why $Bi_5Nb_3O_{15}$ adopts this specific structure presenting structural distortions localized near CSPs instead of having infinite continuous layers of octahedra with strong distortions. $Bi_5Nb_3O_{15}$ is unique among Aurivillius-like phases in that the compositions corresponding to $p = 1$ ($[Bi_2NbO_6]^-$) and $p = 2$ ($[Bi_3Nb_2O_9]^+$) are not charge-neutral and, hence, do not exist as separate phases. $Bi_5Nb_3O_{15}$ is not the usual mixed-layer Aurivillius intergrowth. It is worth noting that, while the stacking sequence along **c** is not uniform, the structure is arranged to produce a regular distribution of the structural blocks (namely, $p = 1$ and 2 Aurivillius-type blocks with finite size) by breaking the layers into slabs of octahedra along **b**. By these means, the system minimizes the number of infinite $[Bi_2O_2]$ slabs forming 2D pseudouniform ordering.[32]

The complexity of the incommensurately modulated structure of $Bi_5Nb_3O_{15}$ is such that a solution from powder diffraction data would have been impossible without electron diffraction techniques, where the truly incommensurate nature of the structure is clearly visible. The proposed structure should

dx.doi.org/10.1021/ic400529s | *Inorg. Chem.* 2013, 52, 6127−6135

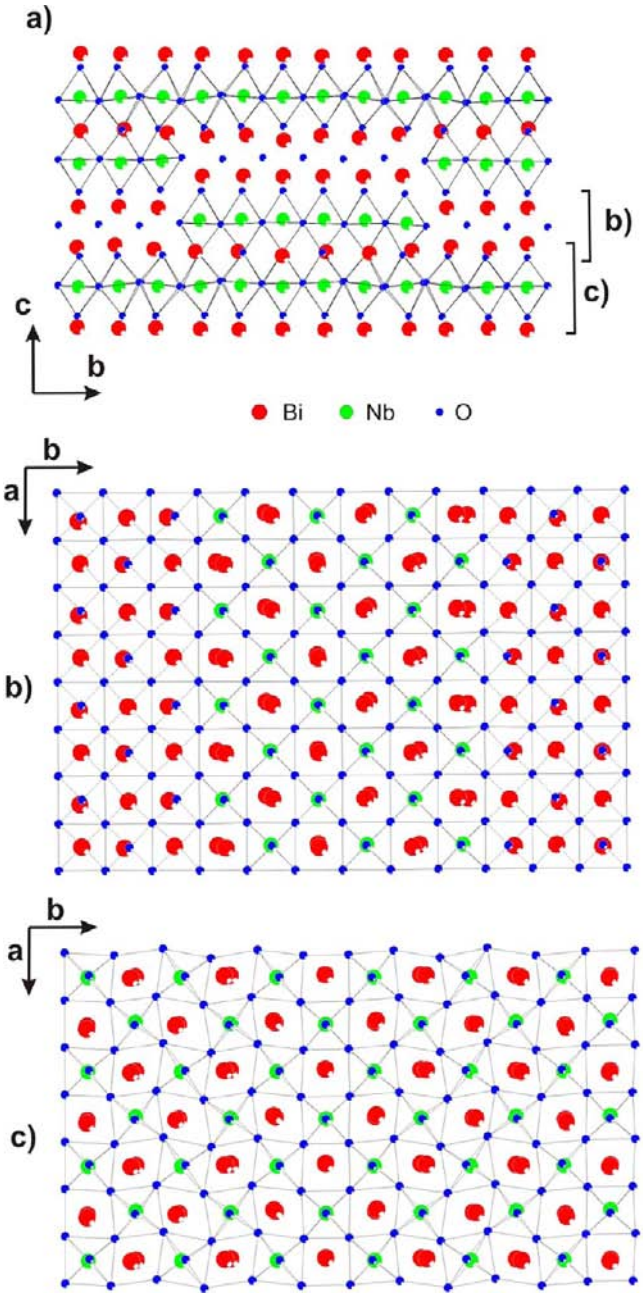

Figure 8. (a) [100] projection of a part of the $Bi_5Nb_3O_{15}$ structure indicating the presence of octahedral tilting along the **a** axis. (b) [001] projection of the discontinuous octahedral layers without noticeable octahedral tilting. (c) [001] projection of the continuous octahedral layers indicating the presence of octahedral tilting along the **c** axis.

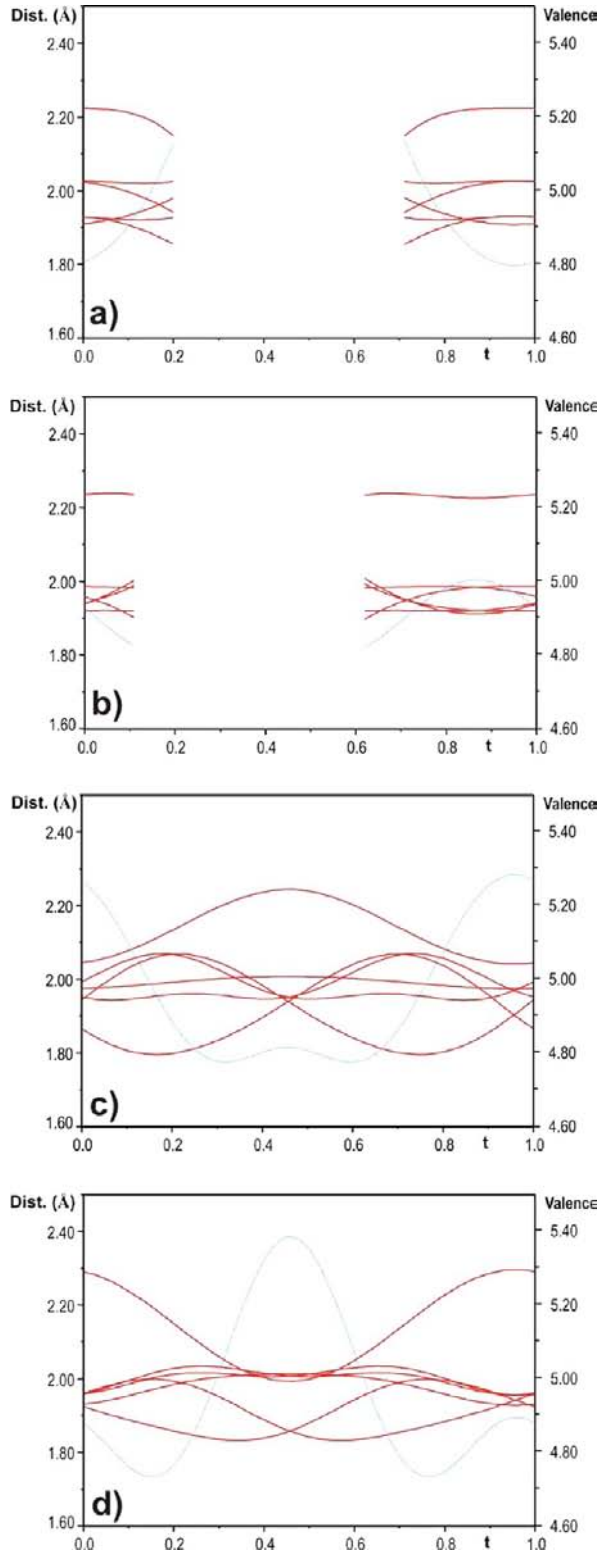

Figure 9. Evolution of Nb−O distances (in red lines) and valences (in blue dotted lines) versus the internal parameter t for (a) Nb1, (b) Nb2, (c) Nb3, and (d) Nb4 atomic positions.

be regarded as an optimization of the PED structure solution against the PXRD data, but the accuracy of the PXRD data is not sufficient to give insight into the fine details. The large amount of satellite reflections obtained in the EDT experiment [~900 for $m = \pm 1$ and ~450 for $m = \pm 2$ independent reflections with $I > 3\sigma(I)$] contrasts strongly with the small number of observed satellite reflections in the PXRD patterns. It is this small number of visible satellites that impedes a more detailed analysis of the incommensurately modulated structure. The weak reflections observed in the powder pattern at $2\theta \approx 10.9°$, 15.1°, 29.2°, and 32.1° seem to be a good signature (see the inset in Figure 5) of the incommensurately modulated nature of $Bi_5Nb_3O_{15}$. These reflections were found as unindexed reflections in the PXRD patterns published by Tahara et al.[14] This indicates that we are most likely dealing with the same material. In the work by Tahara et al., the authors refined the compound as being a conventional mixed-layer Aurivillius structure isostructural to $Bi_5Ti_{1.5}W_{1.5}O_{15}$[8] and $Bi_5TiNbWO_{15}$,[9]

dx.doi.org/10.1021/ic400529s | Inorg. Chem. 2013, 52, 6127−6135

but with space group *Pnc*2 and a unit cell volume of half of what is found for the latter two compounds.

CONCLUSION

The crystal structure of the 1D incommensurately modulated phase $Bi_5Nb_3O_{15}$ has been solved by precession EDT using ab initio phasing by charge flipping. $Bi_5Nb_3O_{15}$ possesses an incommensurately modulated structure with discontinuous modulation functions in which heavy scatterers are present. The structure solution could be obtained by direct interpretation of the charge-flipping output assisted with the basic knowledge of the crystal chemistry of the system under investigation. The (3 + 1)D structure is further validated by a refinement against PXRD, which confirmed the model derived from the electron diffraction data. $Bi_5Nb_3O_{15}$ does not have a conventional mixed-layer Aurivillius-type structure, as previously reported from PXRD and neutron powder diffraction,[14] even though it contains structural elements, namely, $[Bi_2O_2]^{2+}$ slabs and perovskite-like blocks, characteristic of Aurivillius phases. In agreement with earlier reports based on TEM investigations,[11,13] the presence of aperiodic crystallographic shear planes along the modulated direction **b** is confirmed, leading to the formation of an original layered structure containing both continuous and discontinuous $[Bi_2O_2]^{2+}$ and perovskite-like octahedral layers. Between shear planes, the stacking of these two structural elements exhibits a nonuniform sequence unprecedented in known Aurivillius phases.

PED has emerged as a major technique for structure solution when single crystals are not available and when conventional X-ray techniques are barely applicable, like for materials with a small diffracting volume[33,34] or with structures too complex to be tackled using powder diffraction techniques only.[35] The present study represents the latter case. The complexity of the incommensurately modulated structure of $Bi_5Nb_3O_{15}$ is such that a solution from powder diffraction data would have been impossible. The present work is, after the structure of η'-$Cu_{3+x}Si$,[19] another example of how incommensurately modulated structures can be solved from PED data only. With the fast development of the method, it becomes evident that structure solution of complex materials can now be performed almost routinely, and the method deserves attention of the material science community.

ASSOCIATED CONTENT

Supporting Information

Results of the PED (3 + 1)D refinement of $Bi_5Nb_3O_{15}$, structures of PED refinement, and differences in terms of distances between the structural model refined against PXRD and PED data. This material is available free of charge via the Internet at http://pubs.acs.org.

AUTHOR INFORMATION

Corresponding Author

*E-mail: philippe.boullay@ensicaen.fr.

Notes

The authors declare no competing financial interest.

ACKNOWLEDGMENTS

The authors thank Maryvonne Hervieu (CRISMAT, Caen) and Juan-Manuel Perez-Mato (Universidad del Pais Vasco, Bilbao) for valuable discussions and constant support. P.B. acknowledges the ODACE project supported by the French National Research Agency (ANR-2011-BS04-004-03).

REFERENCES

(1) Aurivillius, B. *Ark. Kemi* **1949**, *1*, 463.
(2) Boullay, P.; Trolliard, G.; Mercurio, D.; Elcoro, L.; Perez-Mato, J. M. *J. Solid State Chem.* **2002**, *164*, 252.
(3) Perez-Mato, J. M.; Aroyo, M. I.; Garcia, A.; Blaha, P.; Schwarz, K.; Schweifer, J.; Parlinski, K. *Phys. Rev. B* **2004**, *70*, 21411.
(4) Boullay, P.; Trolliard, G.; Mercurio, D.; Elcoro, L.; Perez-Mato, J. M. *J. Solid State Chem.* **2002**, *164*, 261.
(5) Elcoro, L.; Perez-Mato, J. M.; Izaola, Z.; Boullay, P.; Mercurio, D. *Ferroelectrics* **2004**, *305*, 79.
(6) Tellier, J.; Boullay, P.; Mercurio, D. *Z. Kristallogr.* **2007**, *22*, 234.
(7) Gopalakrishnan, J.; et al. *J. Solid State Chem.* **1984**, *55*, 101.
(8) Tellier, J.; Boullay, P.; Créon, N.; Mercurio, D. *Solid State Sci.* **2005**, *7*, 1025.
(9) Snedden, A.; Charkin, D. O.; Dolgikh, V. A.; Lightfoot, P. *J. Solid State Chem.* **2005**, *178*, 180.
(10) Zhou, W.; Jefferson, D. A.; Thomas, J. M. *Proc. R. Soc. London, Ser. A* **1986**, *406*, 173.
(11) Zhou, W.; Jefferson, D. A.; Thomas, J. M. *Geophys. Monograph.* **1989**, *45*, 113.
(12) Ling, C. D.; et al. *J. Solid State Chem.* **1998**, *137*, 42.
(13) Ling, C. D. *J. Solid State Chem.* **1999**, *148*, 380.
(14) Tahara, S.; Shimada, A.; Kumada, N.; Sugahara, Y. *J. Solid State Chem.* **2007**, *180*, 2517.
(15) Kolb, U.; Gorelik, T.; Kubel, C.; Otten, M. T.; Hubert, D. *Ultramicroscopy* **2007**, *107*, 507.
(16) Vincent, R.; Midgley, P. A. *Ultramicroscopy* **1994**, *53*, 271−282.
(17) Palatinus, L. *PETS—program for analysis of electron diffraction data*; Institute of Physics of the AS CR:Prague, Czechia, 2011.
(18) Petricek, V.; Dusek, M.; Palatinus, L. *Jana2006: Structure Determination Software Programs*; Institute of Physics: Praha, Czech Republic, 2006.
(19) Palatinus, L.; Klementova, M.; Drinek, V.; Jarosova, M.; Petricek, V. *Inorg. Chem.* **2011**, *50*, 3743.
(20) Kolb, U.; Gorelik, T.; Otten, M. T. *Ultramicroscopy* **2008**, *108*, 763.
(21) Palatinus, L.; Chapuis, G. *J. Appl. Crystallogr.* **2007**, *40*, 786.
(22) Palatinus, L.; van der Lee, A. *J. Appl. Crystallogr.* **2008**, *41*, 975.
(23) Takenaka, T.; Komura, K.; Sakata, K. *Jpn. J. Appl. Phys.* **1996**, *35*, 5080.
(24) Zhuk, N. A.; Piir, I. V. *Inorg. Mater.* **2008**, *44*, 1362.
(25) Stokes, H. T.; Campbell, B. J.; van Smaalen, S. *Acta Crystallogr., Sect. A* **2011**, *67*, 45.
(26) Hervieu, M.; Caldes, M. T.; Cabrera, S.; Michel, C.; Pelloquin, D.; Raveau, B. *J. Solid State Chem.* **1995**, *119*, 169.
(27) Hervieu, M.; Pérez, O.; Groult, D.; Grebille, D.; Leligny, H.; Raveau, B. *J. Solid State Chem.* **1997**, *129*, 214.
(28) Suarez, D. Y.; Reaney, I. M.; Lee, W. E. *J. Mater. Res.* **2001**, *11*, 3139.
(29) Blake, S. M.; Falconer, M. J.; McCreedy, M.; Lightfoot, P. *J. Mater. Chem.* **1997**, *7*, 1609.
(30) Tellier, J.; Boullay, P.; Manier, M.; Mercurio, D. *J. Solid State Chem.* **2004**, *177*, 1829.
(31) Tellier, J.; Boullay, P.; Ben Jennet, D.; Mercurio, D. *Solid State Sci.* **2008**, *10*, 177.
(32) Gonzalez, S.; Perez-Mato, J. M.; Elcoro, L.; Garcia, A. *Phys. Rev. B* **2011**, *84*, 184106.
(33) Kverneland, A.; Hansen, V.; Vincent, R.; Gjonnes, K.; Gjonnes, J. *Ultramicroscopy* **2006**, *106*, 492.
(34) Boullay, P.; Dorcet, V.; Perez, O.; Grygiel, C.; Prellier, W.; Mercey, B.; Hervieu, M. *Phys. Rev. B* **2009**, *79*, 184108.
(35) Xie, D.; Baerlocher, C.; McCusker, L. B. *J. Appl. Crystallogr.* **2008**, *41*, 1115.